ACS APPLIED MATERIALS & INTERFACES

Research Article

www.acsami.org

Graphene/Phase Change Material Nanocomposites: Light-Driven, Reversible Electrical Resistivity Regulation via Form-Stable Phase Transitions

Yunming Wang,[†,§] Hongyi Mi,[‡,§] Qifeng Zheng,[†] Zhenqiang Ma,*[,‡] and Shaoqin Gong*[,†]

[†]Department of Biomedical Engineering, Wisconsin Institute for Discovery, and Materials Science Program, University of Wisconsin−Madison, Madison, Wisconsin 53706, United States,

[‡]Department of Electrical and Computer Engineering, University of Wisconsin−Madison, Wisconsin 53706, United States

Supporting Information

ABSTRACT: Innovative photoresponsive materials are needed to address the complexity of optical control systems. Here, we report a new type of photoresponsive nanomaterial composed of graphene and a form-stable phase change material (PCM) that exhibited a 3 orders of magnitude change in electrical resistivity upon light illumination while retaining its overall original solid form at the macroscopic level. This dramatic change in electrical resistivity also occurred reversibly through the on/off control of light illumination. This was attributed to the reversible phase transition (i.e., melting/recrystallization) behavior of the microscopic crystalline domains present in the form-stable PCM. The reversible phase transition observed in the graphene/PCM nanocomposite was induced by a reversible temperature change through the on/off control of light illumination because graphene can effectively absorb light energy and convert it to thermal energy. In addition, this graphene/PCM nanocomposite also possessed excellent mechanical properties. Such photoresponsive materials have many potential applications, including flexible electronics.

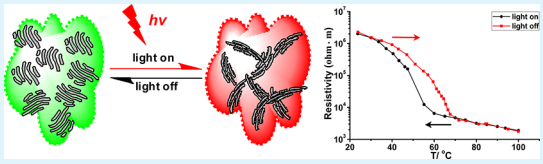

KEYWORDS: *photoresponsive, reversible electrical resistivity, graphene, form-stable phase change material, polymer nanocomposites*

INTRODUCTION

Materials with tunable electrical conductivities can be used for many applications such as switching,[1−3] storage,[4] and sensing[5,6] devices. Compared to inorganic materials, organic materials offer a number of advantages including easier processing and integration for large area electronics, lower cost, and better physical flexibility.[6−8] Polymer nanocomposites, formed by mixing polymers with various types of nanoparticles, have been extensively investigated for many applications.[9,10] The electrical conductivities of polymer nanocomposites containing conductive nanoparticles typically decrease with temperature and often exhibit a sharp drop near the polymer melting points. Beyond the polymer melting points, the electrical conductivities of the nanocomposites typically increase with temperature.[8] While many studies have clearly demonstrated that electrical conductivities of certain polymer nanocomposites can be regulated via temperature,[8] there are a number of limitations, including the following: (1) Drastic conductivity changes occur near the melting temperatures of the polymers, thereby limiting their application due to potential leakage problems. (2) Electrical conductivity is typically lower at elevated temperatures. (3) Reversible change of electrical conductivity is difficult to harness reproducibly. (4) For certain applications, it may be impossible or less desirable to achieve direct temperature control using thermal devices, such as an oven or hot plate, making it necessary to employ remotely controlled photosensitive materials.

To address these challenges, we have developed a family of unique graphene/form-stable phase change material (PCM) nanocomposites exhibiting reversible, dramatic changes in electrical conductivity induced by light illumination. Light-driven materials allow for the control of material properties remotely and reversibly. During the phase change process, form-stable PCMs retain their solid form at the macroscopic level, while the microscopic crystalline regions undergo crystalline-to-amorphous or solid-to-liquid transitions. Consequently, form-stable PCMs do not experience any apparent changes in their physical dimensions at the macroscopic level during phase transition.

For this study, the PCM was synthesized from polyethylene glycol (PEG) and triphenylmethanetriisocyanate (TTI) via a condensation polymerization reaction that did not generate any small molecule byproducts. Meanwhile, graphene, a crystalline form of carbon that is one atom thick, has many desirable properties including a large surface area,[11] excellent chemical stability,[12] superior electrical[13,14] and thermal conductivities,[15−19] and unique optical properties.[20−22] For instance, graphene can effectively absorb photons and subsequently convert optical energy to thermal energy.[23] For this study, functionalized graphene was uniformly dispersed in the PCM and was used as light-driven nanoheaters for the graphene/

Received: November 4, 2014
Accepted: January 14, 2015
Published: January 14, 2015

DOI: 10.1021/am507700r
ACS Appl. Mater. Interfaces 2015, 7, 2641−2647

PCM nanocomposites to induce the form-stable phase transition. Moreover, graphene was also used as an electrically conductive nanofiller for the insulating PCM matrix. The resulting graphene/form-stable PCM nanocomposite can provide an attractive medium for light-driven, temperature-regulated electrical properties through form-stable phase transitions. Specifically, up to 3 orders of magnitude change in electrical resistivity was observed reversibly and reproducibly through the control of on/off switches of light irradiation. Furthermore, the change of magnitude in electrical resistivity can be adjusted by the concentration of the graphene. The graphene/PCM nanocomposites also showed desirable mechanical properties. Thus, these unique graphene/PCM nanocomposites could be used for various applications including flexible photoresponsive electronics.

RESULTS AND DISCUSSION

The compositions of the PCM and graphene/PCM nanocomposites employed for this study are shown in Table 1. The

Table 1. Sample Identification and Nanocompositions

sample	composition
PCM	PEG 20000/TTI = 3:2[a]
1 wt % graphene/PCM	graphene/PCM = 1:100[b]
3 wt % graphene/PCM	graphene/PCM = 3:100
5 wt % graphene/PCM	graphene/PCM = 5:100
7 wt % graphene/PCM	graphene/PCM = 7:100
10 wt % graphene/PCM	graphene/PCM = 10:100

[a]Molar ratios of polyethylene glycol (PEG) and triphenylmethane-triisocyanate (TTI). [b]Weight ratios of surface-functionalized graphene to PCMs.

PCM was synthesized by reacting TTI with polyethylene glycol (PEG 20 kDa). Although graphene possesses many unique properties,[15,24−26] it is a challenge to uniformly disperse the graphene nanosheets into polymer matrixes, which has hindered its application.[27,28] To improve the dispersion of graphene in PCM, we introduced nitrophenyl groups onto the graphene surfaces in this study.[27] The graphene loading content varied from 1 to 10 wt % in the PCM matrix. Structural characterization of the PCM, graphene, and graphene/PCM nanocomposites are shown in Figures S1 and S2 (Supporting Information). As shown in Figure 1a,b, the SEM image of the graphene/PCM composite shows that the surface-functionalized graphene nanosheets were uniformly distributed in the PCM, while the TEM images show that the graphene nanosheets were mostly distributed at the grain boundaries of the PCM matrix that likely consisted of PEG crystalline microdomains. The uniform graphene dispersion shown in SEM was mainly attributed to the strong van der Waals forces present among PCM, toluene, and the nitrophenyl groups of the surface-functionalized graphene.[29−31]

Figure 1c shows the ultraviolet−visible-near-infrared (UV−vis-NIR) absorbance spectra of the PCM and graphene/PCM nanocomposite films. In contrast to the PCM fillm, the graphene/PCM nanocomposite film exhibited almost complete absorbance throughout the UV−vis-NIR range due to the presence of 5 wt % graphene in the composites. More importantly, graphene effectively converted the absorbed optical energy into heat, thereby providing the thermal energy needed to drive the phase transition of PCMs as demonstrated by the XRD analysis described below.[27]

The XRD spectra of the PEG, PCM, and graphene/PCM composites are shown in Figure 2. As shown in Figure 2a, sharp and intense diffraction peaks of PEG were observed at 2θ = 19.12 and 23.24° for all three samples. This finding indicated that PEG crystalline phases were also present in the PCM and graphene/PCM composites.[27,32]

To further investigate the effect of light irradiation on the PEG crystalline structure in the 5 wt % graphene/PCM composite, a series of XRD scans was performed on the composite with light irradiation on (Figure 2b) and off (Figure 2c). Under light irradiation, the intensities of the two PEG diffraction peaks from the graphene/PCM composite decreased rapidly and finally became a broad weak peak, suggesting that PEG phase transition occurred and the PEG crystalline domains were converted to an amorphous liquid state at the micro level. As evidenced by the UV−vis-NIR analysis, graphene in the graphene/PCM composites effectively absorbed the light, and consequently, the absorbed optical energy was converted to thermal energy, raising the temperature (room temperature to 100 °C) of the nanocomposites and causing the phase transition of the PEG crystalline domains.[33] Conversely, this broad peak gradually transformed into two sharp diffraction peaks after the light source was removed, which caused a decline in temperature, thereby triggering the PEG recrystallization process (Figure 2c). This observation illustrates that light can be an effective stimulus for reversibly controlling the phase transition behavior of the PEG crystalline microdomain in graphene/PCM nanocomposites. Figure 2d shows polarized light microscopy images of the PCM film at different temperatures during the cooling process. The crystalline PCM had a typical spherulite morphology.

The differential scanning calorimetry (DSC) curves of the PEG, PCM, and graphene/PCM composites are shown in Figure S3 (Supporting Information), and the enthalpies of the PEG phase transitions (i.e., the melting and recrystallization processes of the PEG crystalline microdomains in the PCM or composite; Figure 2d) were calculated and are listed in Table 2. The difference between the enthalpies of the PCM and graphene/PCM composites was relatively small, and the enthalpies of PCM and graphene/PCM composites were significantly lower than that of the pure PEG. For instance, the melting enthalpies of PEG 20 kDa, PCM, and 5 wt % graphene/PCM composites were 178.5, 110.5, and 102.5 J/g, respectively. The reduction in the degree of PEG crystallinity observed in PCM and graphene/PCM composites in comparison with PEG alone may be partially attributed to the interference and restriction of PEG crystallization by the other components in the PCM and graphene/PCM composites, including the TTI aromatic rings and the graphene. For instance, the melting enthalpies of the graphene/PCM composites generally showed a decreasing trend with an increasing graphene content (i.e., from 110.5, 108.2, 107.1, 102.5, 101.9, to 94.7 J/g corresponding to 0, 1, 3, 5, 7, and 10 wt % graphene, respectively). In terms of the phase transition temperatures (i.e., the melting (T_m) and recrystallization (T_c) temperatures), there was no consistent or significant change between the PCM and the graphene/PCM nanocomposites.

Figure 3 shows the large reversible change of electrical resistivity during the phase transition process under light irradiation. As the temperature increased from room temperature to 100 °C upon light irradiation, the electrical resistivity of the 5 wt % graphene/PCM composite decreased by 3 orders of magnitude, and most of the reduction in electrical resistivity

DOI: 10.1021/am507700r
ACS Appl. Mater. Interfaces 2015, 7, 2641−2647

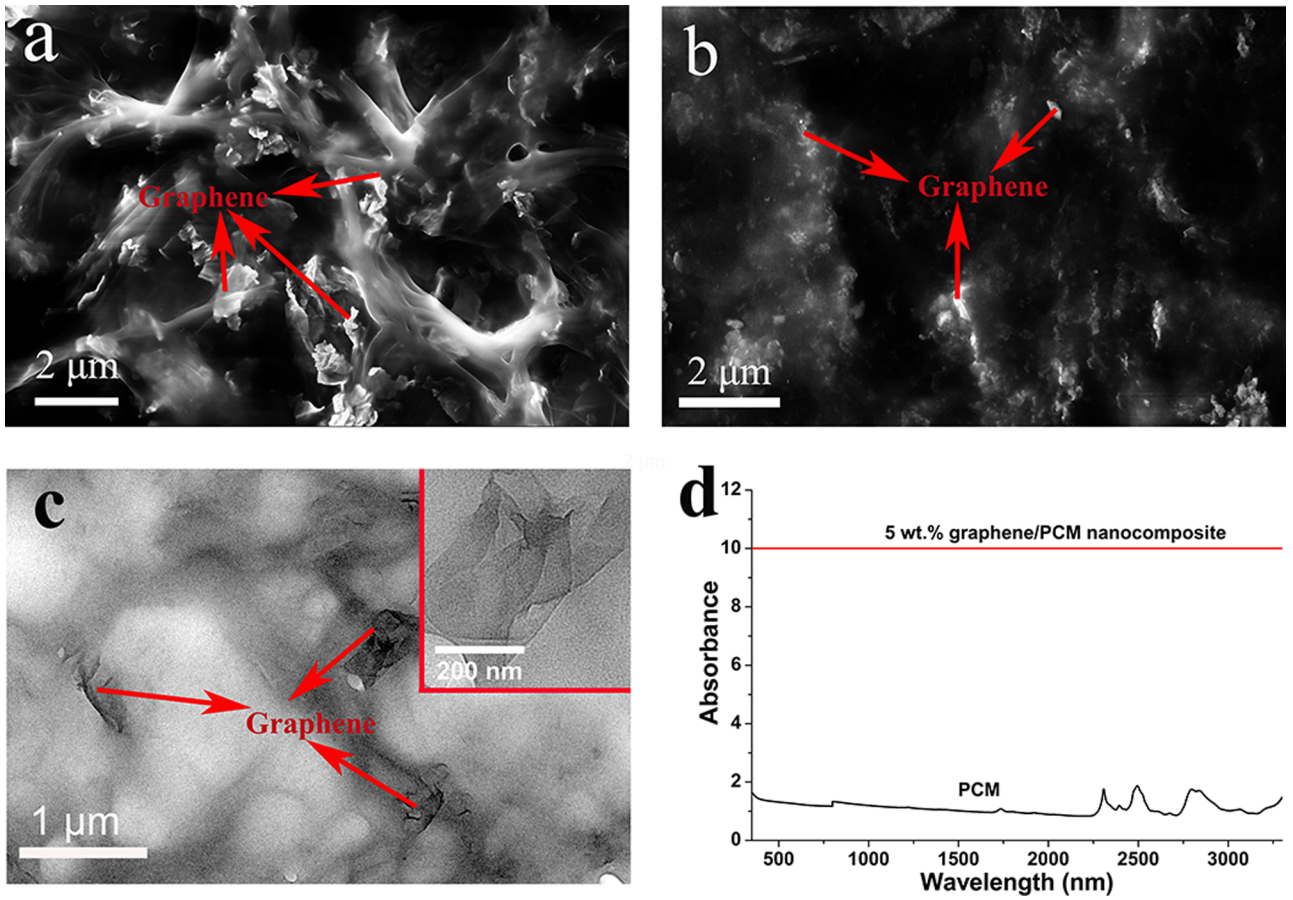

Figure 1. (a) Top-view SEM image of the 5 wt % graphene/PCM nanocomposite film. (b) Cross-sectional SEM image of the 5 wt % graphene/PCM nanocomposite film. (c) TEM image of the 5 wt % graphene/PCM nanocomposite; (inset) TEM image of graphene in 5 wt % graphene/PCM nanocomposite. (d) UV−vis-NIR absorbance spectra of the PCM (thickness of 0.36 mm) and 5 wt % graphene/PCM nanocomposites (thickness 0.12 mm).

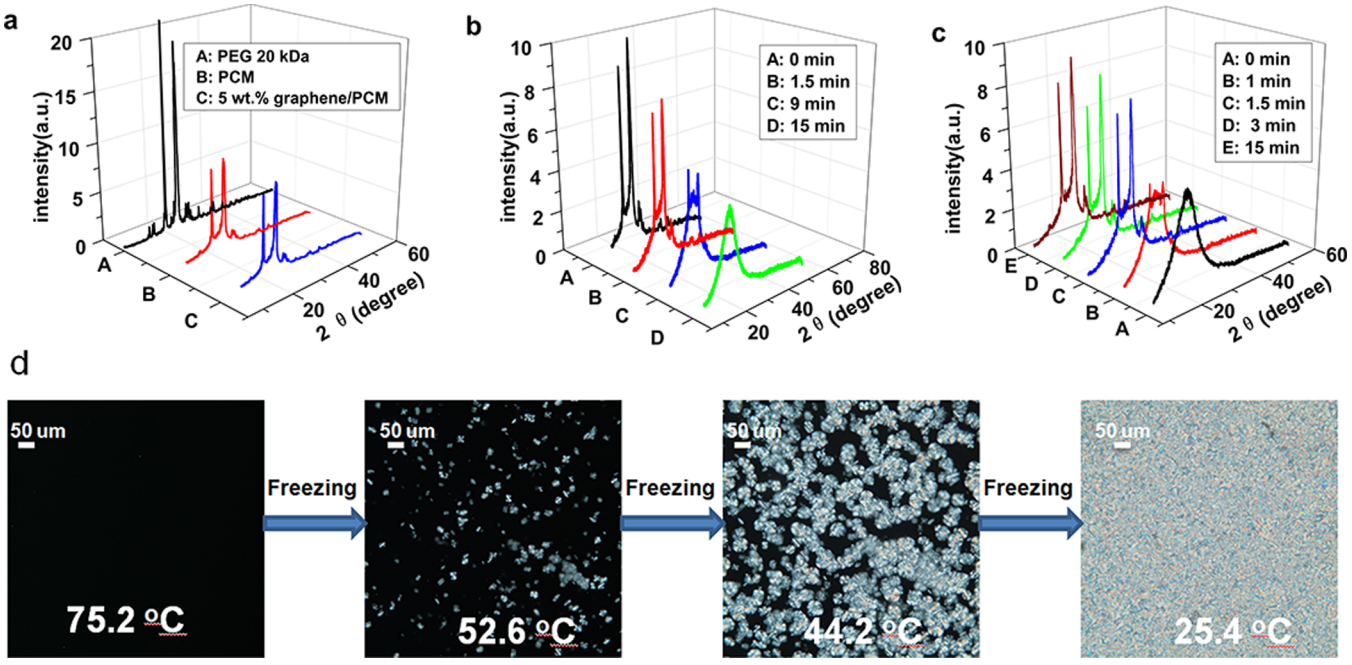

Figure 2. (a) XRD spectra of the PEG (20 kDa), PCM, and graphene/PCM nanocomposite. (b) Series of XRD spectra of the 5 wt % graphene/PCM nanocomposite subjected to white light irradiation (12.5 mW/cm^2). (c) Series of XRD spectra of the 5 wt % graphene/PCM nanocomposite after removing the light irradiation. (d) Polarized microscope images of the PCM during the cooling process.

DOI: 10.1021/am507700r
ACS Appl. Mater. Interfaces 2015, 7, 2641−2647

Table 2. Phase-Change Behaviors of the PEG 20 kDa, PCM, and Graphene/PCM Nanocomposites

samples	phase transition	ΔH (J/g) heating cycle	ΔH (J/g) cooling cycle	T_m (°C) heating cycle	T_c (°C) cooling cycle
PEG 20 kDa	solid−liquid	178.5	179.1	66.9	40.1
PCM	form-stable	110.5	110.9	66.2	42.4
1 wt % graphene/PCM	form-stable	108.2	108.6	64.3	44.8
3 wt % graphene/PCM	form-stable	107.1	108.3	64.2	48.1
5 wt % graphene/PCM	form-stable	102.5	102.3	64.6	45.1
7 wt % graphene/PCM	form-stable	101.3	99.1	65.6	46.2
10 wt % graphene/PCM	form-stable	94.2	93.1	65.3	46.8

occurred during the phase transition process (44−65 °C; Figure 3c, red line). Similarly, the electrical resistivity increased by 3 orders of magnitude upon recrystallization during cooling after removing the light source (Figure 3c, black line). More importantly, the dramatic change in electrical resistivity within the phase transition region was achieved, while the graphene/PCM composite film retained its overall dimensions in its solid form during the entire heating and cooling processes. In other words, unlike the PEG film, which changed from solid phase to liquid phase during phase transition, both PCM and graphene/PCM composite films kept their macroscopic solid state during phase transition, a desirable characteristic of form-stable phase transition materials, as shown in Figure S4 (Supporting Information).

Typically, the electrical resistivity of polymer nanocomposites increases with temperature, which is referred to as the positive temperature coefficient (PTC) effect and has been explained using the conducting path network, tunneling effect, electric field emission, and thermal expansion effect.[6,8,34−37] Under rare occasions, as reported here, the electric resistivity decreases with temperature, which is referred to as the negative temperature coefficient (NTC) effect and has been linked to reaggregation or redistribution of conductive fillers above the polymer melting point.[8,38] Whether the PTC or NTC effect dominates in a polymer nanocomposite depends on many factors including the type, morphology, surface chemistry, dispersion of the fillers, the intrinsic properties of the polymer matrixes, as well as the interaction between the filler and the polymer matrix.[8] There is still a significant lack of understanding regarding the mechanism of the NTC effect.[8] In this study, the drastic change in electrical conductivity/resistivity observed during phase transition is mainly attributed to the internal stress generated during the phase transition that could modulate the electrical contact resistance and lead to a large contrast in the electrical resistivity.[5] As shown in Figure 1, graphene nanosheets were uniformly distributed within the graphene/PCM composites according to SEM analysis and mostly along the grain boundaries of the insulating PCM matrix according to TEM analysis. It is likely that a conducting graphene network was not formed at room temperature due to the encapsulation of these graphene nanosheets by the insulating PCM matrix, thereby leading to a high electrical resistivity. We believe that upon light irradiation, the PEG crystalline microdomains melted, induced localized volume expansion, and generated internal stress, which subsequently enhanced the probability of forming a conductive graphene network and thus drastically reduced the electrical resistivity. Previous studies have demonstrated that annealing carbon/polymer nanocomposites induced the formation of carbon nanotubes or graphene aggregates, leading to a significant increase in electrical conductivity.[39,40] In contrast, during the cooling process with the light irradiation off, the recrystallization of the PEG crystalline microdomains eliminated the

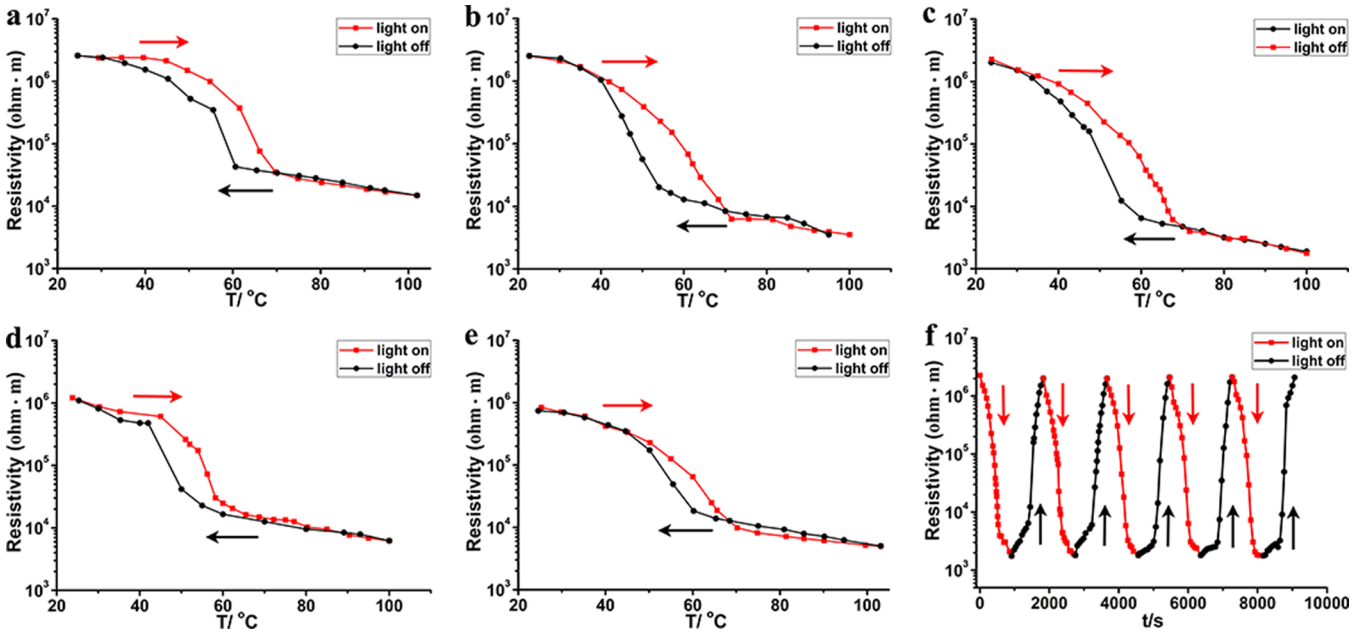

Figure 3. Change in electrical resistivity as a function of temperature induced by light irradiation: (a) 1 wt % graphene/PCM nanocomposite, (b) 3 wt % graphene/PCM nanocomposite, (c) 5 wt % graphene/PCM nanocomposite, (d) 7 wt % graphene/PCM nanocomposite, (e) 10 wt % graphene/PCM nanocomposite, and (f) 5 cyclic electrical resistivity measurements for the 5 wt % graphene/PCM nanocomposite.

DOI: 10.1021/am507700r
ACS Appl. Mater. Interfaces 2015, 7, 2641−2647

internal stress generated during the melting process, which may have also reduced the probability of forming a conductive graphene network and hence induced a drastic increase in electrical resistivity. Outside the phase transition region, the microstructure of the composites was stabilized, and thus, less change in electrical resistivity was observed. Additionally, as shown in Figure 3, the electrical resistivities of the graphene/PCM composites with different graphene concentrations (e.g., 1, 3, 7, and 10 wt %) demonstrated a similar trend as the graphene/PCM composite with 5 wt % graphene (Figure 3c). Furthermore, as expected, the electrical resistivities of the graphene/PCM composites at room temperature decreased with the graphene content (i.e., 2.59×10^6, 2.41×10^6, 2.02×10^6, 1.21×10^6, and 8.38×10^5 Ω·m, corresponding to 1, 3, 5, 7, and 10 wt % graphene, respectively). However, the magnitude of change in electrical resistivity among these graphene/PCM varied significantly. The magnitude of change in electrical resistivity was 174, 783, 1100, 195, and 167 times, respectively, corresponding to 1, 3, 5, 7, and 10 wt % graphene content in the graphene/PCM composites. In other words, the magnitude of change in electrical resistivity initially increased and then decreased with the graphene content. This finding may have been because the electrical conductivity of the graphene/PCM composites were most sensitive to structural and internal stress changes when the graphene loading content was close to the electrical percolation threshold of the composites.[13]

To investigate the reproducibility of the reversible electrical resistivity regulation of the unique graphene/PCM composites, the electrical resistivities of the 5 wt % graphene/PCM composite during five cycles of the melting−recrystallization processes induced by light irradiation were measured and are shown in Figure 3f. The 5 wt % graphene/PCM composites demonstrated reliable reproducibility in achieving light-driven reversible electrical regulation for five heating−cooling cycles, suggesting that the composite has excellent thermal stability within the range of temperatures tested as confirmed by the thermogravimetric analysis (TGA) below. As such, these graphene/PCM composites have a potential for long-term durable applications.

Thermal stability is of vital importance for polymers and polymer composites. TGA was used to study the thermal stability of PEG, PCM, and graphene/PCM composites. Figure 5S (Supporting Information) shows the TGA curves, as well as the first derivatives of the TGA curves (i.e., DTG curves), for these three materials. The thermal stability of the graphene/PCM decreased in comparison with the PCM. For example, the temperature corresponding to a 5 wt % weight loss in the PCM (355.6 °C) was higher than that of graphene/PCM (338.1 °C). The most significant degradation took place within the temperature range 372 to 406 °C, which was due to the exothermic degradation and decomposition of the PEG chains.[27] The amount of char yielded after 600 °C for PEG, PCM, and 5 wt % graphene/PCM composites was 0.3%, 0.4%, and 5.4%, respectively. The larger amount of char yield observed in the graphene/PCM can be attributed to the 5 wt % graphene present in the composites.

To study the mechanical properties of the graphene/PCM composite, we carried out tensile tests according to ASTM D882, and the results are shown in Table 3. Both the tensile strength and strain-at-break of the 5 wt % graphene/PCM decreased in comparison with PCM, which might have been due to the weak interactions between the graphene and the polymer matrix. However, the graphene/PCM nanocomposite still exhibited remarkable flexibility (with a strain-at-break of 1151%) and good tensile strength (16.98 MPa) and modulus (57.26 MPa).

Table 3. Mechanical Properties of the PCM and 5 wt.% Graphene/PCM Nanocomposites

samples	tensile strength at break (MPa)	tensile strain (extension) at break (mm/mm)	Young's modulus (E-modulus) (MPa)
PCM	20.45 ± 1.2	12.27 ± 1.1	57.79 ± 0.8
5 wt % graphene/PCM	16.98 ± 1.2	11.51 ± 0.4	57.26 ± 0.9

CONCLUSIONS

In conclusion, graphene/PCM nanocomposites capable of light-driven regulation of electrical conductivities via form-stable phase transitions were designed and synthesized. These composites demonstrated outstanding regulation of electrical resistivity (up to 3 orders of magnitude) reversibly and reproducibly, as well as excellent mechanical stretchability and thermal stability. Therefore, these composites may yield a number of potential applications in areas such as flexible photoresponsive switching, sensing, and storage devices.

METHODS

Materials. Polyethylene glycol (PEG 20 kDa) was purchased from Sigma-Aldrich (St. Louis, MO) and was dried at 80 °C under high vacuum (0.012 MPa) for 48 h before use. Analytical grade toluene (Fisher Scientific, Bellefonte, PA) was dried for 48 h using a 5 Å molecular sieve and then distilled prior to use. The triphenylmethane-triisocyanate (TTI, BOC Sciences, Shirley, NY) and dibutyltin dilaurate (DBT, Alfa Aesar, Ward Hill, MA) were used as received. N-dimethylformamide (DMF) and tetrahydrofuran (THF) were purchased from Sigma-Aldrich (St. Louis, MO). Natural graphite powder was purchased from Fisher Scientific (Bellefonte, PA). All other reagents were of analytical grade.

Graphene. Graphene oxide (GO) was synthesized from natural graphite powder using the modified Hummer's method.[41,42] GO (100 mg) and deionized (DI) water (10 mL) were placed in a 250 mL round-bottom flask and the mixture was sonicated for 1 h. After that, 90 mL DMF was added into the flask and the mixture was sonicated for another 2 h. Then, the mixture was centrifuged at 4000 rpm to remove nondispersed particles and the homogeneous supernatant dispersion was collected. Subsequently, 1 ml of hydrazine was added to the supernatant dispersion. The mixture was refluxed in a water bath around 85 °C for 24 h. Finally, the resulting reactive mixture was filtered and washed three times by 30 mL DMF and 45 mL DI water, respectively.

Synthesis of Surface-Functionalized Graphene. Graphene was functionalized with 4-nitrophenyl moieties according to a method described in the literature.[43,44] The synthetic process for preparing the surface-functionalized graphene is shown in Scheme 1. Functionalization of graphene was conducted by dispersing 100 mg of graphene in 50 mL of DI water, adding 10 mmol 4-nitroaniline, followed by 10 mmol sodium nitrite, and finally 12 mL of concentrated hydrochloric acid. The mixture was ultrasonicated at 300 W for 4 h at 55 °C and stirred overnight at ambient temperature. It was then filtered and washed successively with water and ethanol. The resulting surface-modified graphene was dried overnight in a vacuum oven.

Synthesis of Form-Stable PCM. The synthesis route for preparing the PCM is shown in Scheme 1. The synthesis reaction was conducted in a flame-dried glassware in an inert nitrogen (N_2) atmosphere. First, 2.0 g of dried PEG 20 kDa, 24.5 mg TTI, and 1 mg of dibutyltin dilaurate (DBT) were mixed in freshly distilled toluene

DOI: 10.1021/am507700r
ACS Appl. Mater. Interfaces 2015, 7, 2641−2647

Scheme 1. Synthesis Scheme for the Surface-Functionalized Graphene, PCM, and the Surface-Functionalized Graphene/PCM Nanocomposites

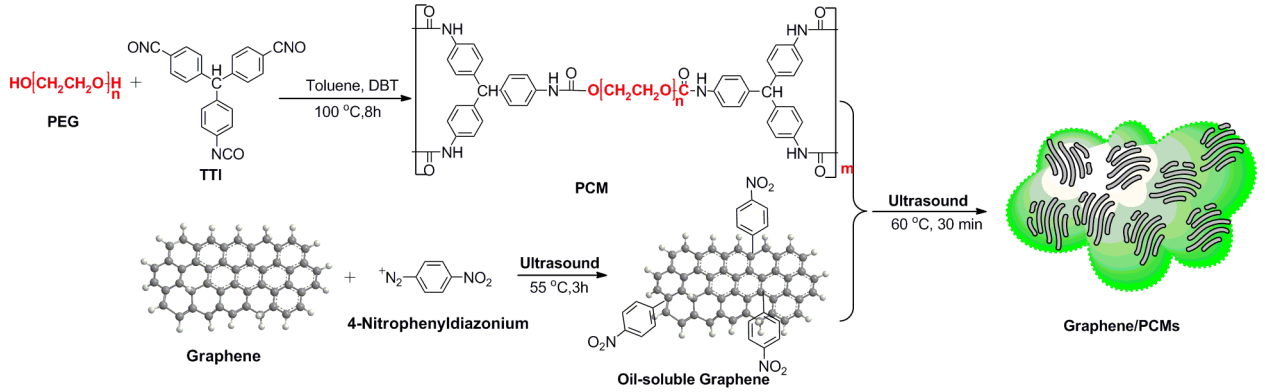

and stirred for 6 h in an N_2 atmosphere at 80 to 85 °C to obtain the hyperbranched polymer (i.e., the form-stable PCM).

Synthesis of the Graphene/PCM Nanocomposites. A specific amount of the surface-modified graphene and the above-obtained PCM toluene solution were mixed and thoroughly stirred (Scheme 1). The mixture was ultrasonicated at 300 W for 30 min at 80 °C to obtain a well-dispersed suspension. The resulting solution was evaporated at 90 °C to produce the graphene/PCM nanocomposite film. The graphene/PCM nanocomposite film was further dried for 48 h at 80 °C under vacuum (0.0014 mbar).

Characterization. The chemical structure of the graphene, PCM, and graphene/PCM nanocomposites were analyzed using a Fourier transform infrared (FTIR) spectrophotometer (Bruker Tensor 27 FT-IR) and a Bruker DPX 300 proton nuclear magnetic resonance spectrometer (^{1}H NMR, DMSO-d_6, with TMS as the internal standard) at room temperature. For the measurement of light-driven electrical resistivity regulation, a Fisher Scientific microscope fiber-optic light (No. 112-562-21) was used as a light irradiation source. An HP4155 semiconductor analyzer was used to measure the electrical resistivity of the samples. A thermometer with K-type thermocouple was used to record the temperature of the samples during light irradiation. Light irradiation was set for the samples to achieve a steady temperature increase/decrease rate (approximately 5 °C/min). A silver wire detector was set underneath the samples in order to measure the temperature accurately. Scanning electron microscopy (SEM, LEO GEMINI 1530 Zeiss, Germany) and transmission emission microscopy (TEM, FEI Tecnai T12) were used to characterize the microstructure of the graphene/PCM nanocomposites. For TEM analysis, the sample (about 50 nm in thickness) was prepared using a microtome (Reichert UltraCut E, Depew, NY). Differential scanning calorimetry (DSC) was performed in an N_2 atmosphere using a Q20 DSC thermal analyzer (TA Instruments, New Castle, DE) from 0 to 80 °C at a heating rate of 5 °C/min and a N_2 flow rate of 20 mL/min. The DSC sample (about 5.0 mg) was stored in a sealed aluminum pan. The latent heat was calculated as the total area under the transition peaks of the graphene/PCM nanocomposites using thermal analysis software. To study the effect of temperature on the dimension/shape of the graphene/PCM nanocomposite films, digital images of these films were taken periodically while they were heated on a hot stage from 30 to 100 °C at a rate of 5 °C/min. The thermal stability of these films were characterized via thermogravimetric analysis (TGA) using a TGA/Q50 thermal analyzer (TA Instruments, New Castle, DE). Approximately 10 mg of the nanocomposite films were heated from 30 to 600 °C at a heating rate of 10 °C/min in an N_2 atmosphere. X-ray diffraction (XRD, Bruker D8-Discovery) analysis was performed on the samples within 5−80° (diffraction angles, 2θ). Prior to the XRD analysis, the time it took to reach a specific temperature (from room temperature to 100 °C) for the sample set on the XRD stage during light irradiation was measured using a thermometer with a K-type thermocouple. Its silver wire detector was put just beneath the sample. According to the irradiation time−temperature correlation obtained from this measurement, the XRD analysis was then carried out on the sample under the same light illumination condition except that the silver wire detector beneath the sample was removed. UV−vis-NIR absorbance was measured using a Varian Cary 5000 Bio UV−visible-NIR spectrophotometer. The tensile properties of the films were characterized according to ASTM: D882 using a universal testing machine (Instron 5967, Grove City, PA). The tensile strain rate was set at 10% min^{-1} for the tests. A Fisher Scientific microscope fiber-optic light (No. 112-562-21) was employed as the illumination source. The polarized optical images for cyrstalline PEG were taken using a polarized light microscope (EN60950, Diagnostic Instruments, Inc., Sterling Heights, MI).

■ ASSOCIATED CONTENT

Supporting Information

Structural analyses, DSC, form-stable properties, and TGA of the PCM and graphene/PCM nanocomposites. This material is available free of charge via the Internet at http://pubs.acs.org.

■ AUTHOR INFORMATION

Corresponding Authors

*E-mail: mazq@engr.wisc.edu. Tel: +1-608-261-1095.
*E-mail: sgong@engr.wisc.edu. Tel: +1-608-316-4311.

Author Contributions

§Y.W. and H.M. contributed equally to this work.

Notes

The authors declare no competing financial interest.

■ ACKNOWLEDGMENTS

The authors are thankful to Mr. Guojun Chen for his help with the TEM analysis and to Mr. Tianliang Zhai for his assistance with the mechanical testing.

■ REFERENCES

(1) Park, W. I.; You, B. K.; Mun, B. H.; Seo, H. K.; Lee, J. Y.; Hosaka, S.; Yin, Y.; Ross, C. A.; Lee, K. J.; Jung, Y. S. Self-Assembled Incorporation of Modulated Block Copolymer Nanostructures in Phase-Change Memory for Switching Power Reduction. *ACS Nano* **2013**, *7*, 2651−2658.

(2) Iimori, T.; Ohta, N. Tuning of Electrical Conductivity by Photoirradiation and Electric Fields. *J. Phys. Chem. C* **2014**, *118*, 7251−7260.

(3) Nanotechnology: Single-Molecule Electric Switch. *Nature* **2013**, *499*, 129−129.

(4) Fu, D. W.; Cai, H. L.; Liu, Y. M.; Ye, Q.; Zhang, W.; Zhang, Y.; Chen, X. Y.; Giovannetti, G.; Capone, M.; Li, J. Y.; Xiong, R. G. Diisopropylammonium Bromide Is a High-Temperature Molecular Ferroelectric Crystal. *Science* **2013**, *339*, 425−428.

DOI: 10.1021/am507700r
ACS Appl. Mater. Interfaces 2015, 7, 2641−2647

(5) Zheng, R.; Gao, J.; Wang, J.; Chen, G. Reversible Temperature Regulation of Electrical and Thermal Conductivity Using Liquid−Solid Phase Transitions. *Nat. Commun.* **2011**, *2*, 289−294.
(6) Welnic, W.; Wuttig, M. Reversible Switching in Phase-Change Materials. *Mater. Today.* **2008**, *11*, 20−27.
(7) Iimori, T.; Ohta, N. Tuning of Electrical Conductivity by Photoirradiation and Electric Fields. *J. Phys. Chem. C* **2014**, *118*, 7251−7260.
(8) Tjong, S. C. Electrical Properties of Polymer Nanocomposites. In *Polymer Composites with Carbonaceous Nanofillers*; Wiley-VCH Verlag GmbH & Co. KGaA: Weinheim, 2012; pp 193−245.
(9) Winey, K. I.; Vaia, R. A. Polymer Nanocomposites. *MRS Bull.* **2007**, *32*, 314−322.
(10) Wing, M. Y.; Zhongzhen, Y.; Xaolin, X.; Qingxin, Z.; Jun, M. A. Polymer Nanocomposites and Their Applications. *HKIE Trans.* **2003**, *10*, 67−73.
(11) Tan, Y. B.; Lee, J.-M. Graphene for Supercapacitor Applications. *J. Mater. Chem. A* **2013**, *1*, 14814−14843.
(12) Lee, S.-K.; Rana, K.; Ahn, J.-H. Graphene Films for Flexible Organic and Energy Storage Devices. *J. Phys. Chem. Lett.* **2013**, *4*, 831−841.
(13) Wu, C.; Huang, X.; Wang, G.; Lv, L.; Chen, G.; Li, G.; Jiang, P. Highly Conductive Nanocomposites with Three-Dimensional, Compactly Interconnected Graphene Networks via a Self-Assembly Process. *Adv. Funct. Mater.* **2013**, *23*, 506−513.
(14) Wang, X.; Xie, W.; Chen, J.; Xu, J.-B. Homo- and Hetero- p−n Junctions Formed on Graphene Steps. *ACS Appl. Mater. Interfaces* **2013**, *6*, 3−8.
(15) Zhu, J.; Zhang, H. N.; Kotov, N. A. Thermodynamic and Structural Insights into Nanocomposites Engineering by Comparing Two Materials Assembly Techniques for Graphene. *ACS Nano* **2013**, *7*, 4818−4829.
(16) O'Hern, S. C.; Boutilier, M. S. H.; Idrobo, J. C.; Song, Y.; Kong, J.; Laoui, T.; Atieh, M.; Karnik, R. Selective Ionic Transport through Tunable Subnanometer Pores in Single-Layer Graphene Membranes. *Nano Lett.* **2014**, *14*, 1234−1241.
(17) Yang, X. W.; Cheng, C.; Wang, Y. F.; Qiu, L.; Li, D. Liquid-Mediated Dense Integration of Graphene Materials for Compact Capacitive Energy Storage. *Science* **2013**, *341*, 534−537.
(18) Xu, P. F.; Dong, L.; Neek-Amal, M.; Ackerman, M. L.; Yu, J. H.; Barber, S. D.; Schoelz, J. K.; Qi, D. J.; Xu, F. F.; Thibado, P. M.; Peeters, F. M. Self-Organized Platinum Nanoparticles on Freestanding Graphene. *ACS Nano* **2014**, *8*, 2697−2703.
(19) Han, S.; Wu, D. Q.; Li, S.; Zhang, F.; Feng, X. L. Porous Graphene Materials for Advanced Electrochemical Energy Storage and Conversion Devices. *Adv. Mater.* **2014**, *26*, 849−864.
(20) Shao, L.; Wang, X.; Xu, H.; Wang, J.; Xu, J.-B.; Peng, L.-M.; Lin, H.-Q. Nanoantenna-Sandwiched Graphene with Giant Spectral Tuning in the Visible-to-Near-Infrared Region. *Adv. Opt. Mater.* **2014**, *2*, 162−170.
(21) Brownson, D. A. C.; Banks, C. E. The Electrochemistry of CVD Graphene: Progress and Prospects. *Phys. Chem. Chem. Phys.* **2012**, *14*, 8264−8281.
(22) Liu, M.; Yin, X.; Ulin-Avila, E.; Geng, B.; Zentgraf, T.; Ju, L.; Wang, F.; Zhang, X. A Graphene-Based Broadband Optical Modulator. *Nature* **2011**, *474*, 64−67.
(23) Chen, L.; Zou, R.; Xia, W.; Liu, Z.; Shang, Y.; Zhu, J.; Wang, Y.; Lin, J.; Xia, D.; Cao, A. Electro- and Photodriven Phase Change Composites Based on Wax-Infiltrated Carbon Nanotube Sponges. *ACS Nano* **2012**, *6*, 10884−10892.
(24) Chua, C. K.; Pumera, M. Regeneration of a Conjugated sp(2) Graphene System through Selective Defunctionalization of Epoxides by Using a Proven Synthetic Chemistry Mechanism. *Chem.—Eur. J.* **2014**, *20*, 1871−1877.
(25) Zhu, J. X.; Yang, D.; Yin, Z. Y.; Yan, Q. Y.; Zhang, H. Graphene and Graphene-Based Materials for Energy Storage Applications. *Small* **2014**, *10*, 3480−3498.
(26) Zhang, K.; Yap, F. L.; Li, K.; Ng, C. T.; Li, L. J.; Loh, K. P. Large Scale Graphene/Hexagonal Boron Nitride Heterostructure for Tunable Plasmonics. *Adv. Funct. Mater.* **2014**, *24*, 731−738.
(27) Wang, Y. M.; Tang, B. T.; Zhang, S. F. Single-Walled Carbon Nanotube/Phase Change Material Composites: Sunlight-Driven, Reversible, Form-Stable Phase Transitions for Solar Thermal Energy Storage. *Adv. Funct. Mater.* **2013**, *23*, 4354−4360.
(28) Zhu, J. H.; Chen, M. J.; He, Q. L.; Shao, L.; Wei, S. Y.; Guo, Z. H. An Overview of the Engineered Graphene Nanostructures and Nanocomposites. *RSC Adv.* **2013**, *3*, 22790−22824.
(29) Schulz-Drost, C.; Sgobba, V.; Gerhards, C.; Leubner, S.; Krick Calderon, R. M.; Ruland, A.; Guldi, D. M. Innovative Inorganic−Organic Nanohybrid Materials: Coupling Quantum Dots to Carbon Nanotubes. *Angew. Chem., Int. Ed.* **2010**, *49*, 6425−6429.
(30) Zhu, J.; Shim, B. S.; Di Prima, M.; Kotov, N. A. Transparent Conductors from Carbon Nanotubes LBL-Assembled with Polymer Dopant with $\pi-\pi$ Electron Transfer. *J. Am. Chem. Soc.* **2011**, *133*, 7450−7460.
(31) Bao, Q.; Zhang, H.; Yang, J.-X.; Wang, S.; Tang, D. Y.; Jose, R.; Ramakrishna, S.; Lim, C. T.; Loh, K. P. Graphene−Polymer Nanofiber Membrane for Ultrafast Photonics. *Adv. Funct. Mater.* **2010**, *20*, 782−791.
(32) Tang, B.; Qiu, M.; Zhang, S. Thermal Conductivity Enhancement of PEG/SiO2 Composite PCM by in Situ Cu Doping. *Sol. Energy Mater. Sol. Cells* **2012**, *105*, 242−248.
(33) Kim, S. A.; Archer, L. A. Hierarchical Structure in Semicrystalline Polymers Tethered to Nanospheres. *Macromolecules* **2014**, *47*, 687−694.
(34) Meyer, J. Glass Transition Temperature As a Guide to Selection of Polymers Suitable for PTC Materials. *Polym. Eng. Sci.* **1973**, *13*, 462−468.
(35) Meyer, J. Stability of Polymer Composites As Positive-Temperature-Coefficient Resistors. *Polym. Eng. Sci.* **1974**, *14*, 706−716.
(36) Klason, C.; Kubát, J. Anomalous Behavior of Electrical Conductivity and Thermal Noise in Carbon Black-Containing Polymers at T_g and T_m. *J. Appl. Polym. Sci.* **1975**, *19*, 831−845.
(37) Al - Allak, H. M.; Brinkman, A. W.; Woods, J. *I−V* Characteristics of Carbon Black-Loaded Crystalline Polyethylene. *J. Mater. Sci.* **1993**, *28*, 117−120.
(38) Ansari, S.; Giannelis, E. P. Functionalized Graphene Sheet—Poly(vinylidene fluoride) Conductive Nanocomposites. *J. Polym. Sci., Part B: Polym. Phys.* **2009**, *47*, 888−897.
(39) Alig, I.; Skipa, T.; Engel, M.; Lellinger, D.; Pegel, S.; Pötschke, P. Electrical Conductivity Recovery in Carbon Nanotube−Polymer Composites after Transient Shear. *Phys. Status. Solidi. B* **2007**, *244*, 4223−4226.
(40) Zhan, Y.; Lavorgna, M.; Buonocore, G.; Xia, H. Enhancing Electrical Conductivity of Rubber Composites by Constructing Interconnected Network of Self-Assembled Graphene with Latex Mixing. *J. Mater. Chem.* **2012**, *22*, 10464−10468.
(41) Hong, T.-K.; Lee, D. W.; Choi, H. J.; Shin, H. S.; Kim, B.-S. Transparent, Flexible Conducting Hybrid Multilayer Thin Films of Multiwalled Carbon Nanotubes with Graphene Nanosheets. *ACS Nano* **2010**, *4*, 3861−3868.
(42) Kotal, M.; Bhowmick, A. K. Multifunctional Hybrid Materials Based on Carbon Nanotube Chemically Bonded to Reduced Graphene Oxide. *J. Phys. Chem. C* **2013**, *117*, 25865−25875.
(43) Lomeda, J. R.; Doyle, C. D.; Kosynkin, D. V.; Hwang, W. F.; Tour, J. M. Diazonium Functionalization of Surfactant-Wrapped Chemically Converted Graphene Sheets. *J. Am. Chem. Soc.* **2008**, *130*, 16201−16206.
(44) Wang, Q. H.; Shih, C.-J.; Paulus, G. L. C.; Strano, M. S. Evolution of Physical and Electronic Structures of Bilayer Graphene upon Chemical Functionalization. *J. Am. Chem. Soc.* **2013**, *135*, 18866−18875.

DOI: 10.1021/am507700r
ACS Appl. Mater. Interfaces 2015, 7, 2641−2647